Grain Boundary Structure and Segregation in Ni- and Al-Rich NiAl

David E. Luzzi*
Department of Materials Science and Engineering
Kyoto University
Sakyo-ku, Kyoto, Japan

R.W. Fonda
Naval Research Laboratory
Washington, DC, USA

and

M. Yan
Los Alamos National Laboratory
Los Alamos, NM, USA

(Received: Jan. 30, 1997 Accepted: Feb. 20, 1997)

Abstract

A combined experimental and theoretical modeling approach utilizing high-resolution electron microscopy (HREM) and atomistic structure calculations has been used to solve the atomic structure of a Σ=5 (310) [001] grain boundary in Ni-rich NiAl. The resultant structure model, which contains nickel antisite defects adjacent to the grain boundary plane, is consistent with the HREM experimental data, was found to be the lowest energy structure at 0K via molecular statics calculations, and was stable at higher temperatures as determined from Monte Carlo calculations. The calculations, employing new N-body empirical potentials which correctly reproduce the point defect properties of NiAl, were then extended to the study of stoichiometric and Al-rich grain boundaries. Segregation of point defects to the boundary is favored in Ni-rich and Al-rich NiAl. In Al-rich NiAl, either Ni vacancies or Al antisite defects may be found at the grain boundary, whereas only Ni constitutional vacancies are favored within the bulk.

1. Introduction

Interface properties often determine the macroscopic properties of a material, as the kinetics of physical processes are typically higher (or lower) at interfaces and interfaces are often the preferred paths for crack propagation. Physical and mechanical properties at the interface are intimately linked to the atomic structure of the interface. In order to gain a full understanding of the effect of interfaces on material properties with the long term goal of developing some predictive capability for material development, it is essential that the understanding of the atomic structure of interfaces be advanced.

An excellent example for the critical importance of interface studies is the high temperature structural intermetallic NiAl. Despite having a low density, good thermal conductivity, and excellent oxidation and corrosion resistance, as well as a higher application temperature than conventional titanium- and nickel-based alloys (1), the intergranular brittleness of NiAl (2) limits current developments of this alloy to single crystal applications. In conventional alloys, intergranular brittle fracture is usually caused by segregation of embrittling impurities to the grain boundary (3). However, the grain boundaries of intermetallic alloys which fracture in an intergranular mode have been shown to be free of such impurities (4, 5, 6, 7, 8). Therefore, these intermetallic alloys have often been considered to be intrinsically brittle. Atomistic calculations have shown that the ordering energy could be a primary factor in causing the intergranular brittleness of intermetallics (9, 10, 11, 12). Simulated grain boundary structures for metals and weakly ordered intermetallic alloys, neither of which exhibit this intrinsic brittleness, are similar to each other in the relaxation of lattice sites at the grain boundary. This relaxation of the grain boundary region may increase the cohesion of the boundary or permit dislocations to be transmitted through the grain boundary,

* Permanent Address:
Department of Materials Science and Engineering
University of Pennsylvania
Philadelphia, PA, USA*

thereby relieving the stress on the boundary. On the other hand, the high ordering energy characteristic of many intermetallic alloys prevents such a relaxation of the grain boundary sites; the structural and chemical characteristics of each grain are preserved up to the grain boundary. This highly ordered grain boundary structure has been shown (13) to inhibit dislocation transmittance across the boundary, which may result in locally elevated stresses at grain boundaries due to the accumulation of dislocations. In addition, these highly ordered structures often exhibit large grain boundary expansions which has been shown to be correlated with a higher grain boundary energy and therefore lower cohesive strength(14). Thus, grain boundaries in strongly ordered materials are likely to be intrinsically more brittle than those in weakly ordered or compositionally disordered materials.

The only technique which can directly observe the internal structure of a grain boundary is high resolution electron microscopy (HREM). The primary disadvantage of HREM is that the actual structure giving rise to a particular HREM image cannot be determined directly from the image. The structure can only be determined by direct comparison between the experimental image and an image simulated from a physically sound model under the same imaging conditions. This highlights the advantages of a synergistic approach combining HREM and atomistic calculations. With HREM, the grain boundary expansion and rigid body displacements (normal to the beam direction) can be accurately measured, providing a first approximation of the grain boundary structure. Complementary atomistic relaxation calculations are then used to determine structural configurations for which the free energy is locally minimized. This is essential in determining physically realistic structures. Finally, detailed comparisons between images calculated from the relaxed structures and the HREM experimental images are used to determine which among the possible stable structures is actually observed. Throughout this iterative process, both the theoretical and experimental treatments tend to be refined through comparison with the complimentary analysis. For example, small shifts in atom positions are often found from atomistic simulation which are beyond the resolving power of the HREM and the comparison with the experimental image can be the final arbiter among two or more relaxed structures whose energies are too close for selection based solely on simulation.

The techniques of HREM and atomistic calculation are also synergistic in a broader sense. The geometrical constraints of both grain misorientation and grain boundary orientation for imaging a grain boundary with HREM limit the applicability of this method to a few special or pure tilt grain boundary configurations. Atomistic calculations have no such geometrical limitations; they can be applied to any grain boundary geometry and misorientation, within the limitations of computation time and the available interatomic potentials. The primary limitation of atomistic calculations is in the construction of accurate interatomic potentials. While the empirical N-body potentials used in this study are founded on many material parameters, accurate reproduction of an experimentally observed structure provides a critical verification of these potentials. If the atomistic relaxation calculations can accurately reproduce an experimentally observed structure, additional atomistic calculations on configurations which are not experimentally accessible will be more credible.

In the present paper, an analysis using the above approach of the effect of non-stoichiometry on the structure of a grain boundary in NiAl is reviewed. The atomic structure of a Σ=5 (310) [001] grain boundary in Ni-rich NiAl was determined by synergistic HREM experimentation and atomistic simulation. The experimental data showed that existing empirical potentials developed for Ni_3Al used in other computer-based studies of NiAl did not correctly treat point defects in this material(15). Namely, existing potentials predicted stable Al antisite defects in contradiction to well-established experimental data based on x-ray diffraction and mass density measurements (see below). New N-body empirical potentials were produced which correctly reproduce the experimentally observed point defect properties of non-stoichiometric NiAl(16). Using these new potentials, a detailed study of the structure of the Σ=5 (310) [001] grain boundary in stoichiometric, Ni-rich and Al-rich NiAl(17) was done. These results are reviewed and the implications for the atomic structure of grain boundaries in strongly-ordered NiAl is

discussed.

Although the effect of non-stoichiometry within the bulk has been well established, there have been few previous examinations of the structure or chemistry of grain boundaries in NiAl (18, 19, 20, 21). In a classic study, Bradley and Taylor determined that non-stoichiometry within the bulk is accommodated by nickel antisite defects in nickel-rich compositions and by compositional vacancies on the nickel sublattice in aluminum-rich compositions(22). Grain boundaries in NiAl were shown to be depleted in aluminum, relative to the surrounding matrix, in a Ni-49%Al alloy(19, 20). Both Chen et al.(18) and Petton and Farkas (21) have conducted atomistic calculation examinations of NiAl grain boundaries using interatomic potentials which had been developed for the Ni_3Al phase (21). The results of Chen et al. (18) indicated that non-stoichiometry in the alloy results in the formation of vacancies of the minority element at the grain boundary while the results of Petton and Farkas (21) showed a strong correlation between the aluminum content of the grain boundary and the grain boundary energy; higher aluminum content raised the grain boundary energy while higher nickel content lowered it. However, as mentioned above, the Ni_3Al interatomic potentials used in these studies are not able to correctly reproduce the material properties of NiAl, primarily due to the very strong Al-Al repulsion inherent in NiAl which was not necessary in the development of the Ni_3Al potentials.

2. Experimental Details

2.1 HREM and Multislice Calculations

The Σ=5 (310) [001] grain boundary examined in this study was prepared from a single crystal of Ni-rich NiAl. Slices of this single crystal were cut parallel to (310) on a Charmilles EDM, then oriented more accurately by mechanical polishing. The slices were then oriented with their [001] directions anti-parallel, which produces the 36.9° rotation between [010] directions necessary for the Σ=5 relationship. The slices were diffusion bonded in this orientation at 280 p.s.i. uniaxial pressure, 1000 °C, and 10^{-5} torr for 3 h in a graphite furnace. HREM foils were prepared by sectioning the resultant bicrystal normal to the common [001] direction, cutting 3 mm discs from these sections, then mechanically thinning the disks to 125 mm. These samples were dimpled in 10% perchloric acid in ethanol at 44 V, then electropolished to perforation in the same solution at 44 V (320 mA) and -25 °C. HREM examination was performed on a JEOL 4000 EX operating at 400 kV. Simulated images of model grain boundary structures were generated using the NUMIS multislice simulation program with C_S= 1.0 mm, beam convergence=2.0 mrad, and focal spread=100 Å FWHM.

2.2 Atomistic Calculation Method

Atomistic relaxation calculations were performed using empirical N-body central force potentials which were constructed within the framework developed by Finnis and Sinclair (23). In this framework, the total energy of a system of N atoms is given by

$$E_{tot} = \frac{1}{2}\sum_{i=1}^{N}\left[\sum_{j\neq i} V_{S_iS_j}(R_{ij}) - \sqrt{\sum_{j\neq i}\Phi_{S_iS_j}(R_{ij})}\right]$$

where the first term represents the energy resulting from the direct interaction between two atoms and the second term represents the *N*-body attractive part of the cohesive energy (24). The two pair potentials, V and Φ, are empirically fitted to the properties of the atomic species S_i and S_j, and R_{ij} represents the separation of atoms i and j. The Ni-Ni potential, which had previously been fitted to the experimentally known lattice parameter, cohesive energy, elastic constants, and vacancy formation energy of pure Ni (25), was adjusted at separations smaller than the nearest neighbor distance (in pure Ni) to reproduce the pressure-volume relationship calculated from the universal equation (26). The Al-Al potential, which had been fitted in a similar fashion(27), was modified to increase the repulsive Al-Al interactions at separations smaller than the nearest neighbor distance. This modification causes the formation of two vacancies on the Ni sites of NiAl to be energetically preferred relative to the formation of an Al antisite defect on the Ni sublattice, in agreement with experimental evidence on Al-rich alloys (22). To develop the Ni-Al potential, Φ_{NiAl} was taken as the geometric mean of the Φ potentials for pure Ni and pure Al, which is consistent with its interpretation in terms of hopping integrals (24). The V_{NiAl} potential was fitted to

reproduce the experimentally known lattice constant, cohesive energy, and elastic constants of the B2-ordered NiAl phase. At atomic separations smaller than the first nearest neighbor distance, the $\mathbf{V}_{NiAl}$ potential was adjusted to comply with the pressure-volume relation calculated from the universal equation (26).

Using these potentials, the energy of a Ni antisite defect on an Al site was calculated to be -0.64 eV, while the energy of an Al antisite defect on a Ni site was determined to be 2.53 eV. The exchange of a Ni atom with an Al atom thus results in an energy increase of 1.89 eV. This barrier to disordering of the B2 lattice has been found to stabilize the B2 structure up to 2000 K (28). The energy calculated for the formation of a vacancy on a Ni site is 1.3 eV. Although this energy is more than one-half the energy of an Al antisite defect, the free energy of two Ni vacancies is lower than that of the Al antisite defect due to configurational entropy effects. These potentials are therefore consistent with the experimental observation of Ni vacancies in Al-rich alloys (22). With these potentials, the B2 structure of the NiAl phase is energetically favored over the L10 structure and the energy of the {110} antiphase boundary is calculated to be 437 mJ/m^2, which is within the experimentally measured range (29). In addition, the properties of the $L1_2$ Ni_3Al phase are reproduced very well with these potentials, even though they were not directly included in the potential fitting. Thus, these potentials can be applied to a wide range of both atomic neighbor environments and compositions in the Ni-Al system, which are often present in the vicinity of defects.

The atomistic relaxation calculations were conducted on geometrically constructed bicrystals of NiAl containing the Σ=5 (310) [001] grain boundary. Various rigid body displacements between the upper and lower grain, including the experimentally observed displacements, were examined in these calculations. In addition, the chemical composition of the grain boundary was varied by introducing vacancies or antisite defects into the initially stoichiometric structures prior to relaxation. The reported grain boundary energies are calculated with respect to the energy of the perfect B2 lattice which contains the same total number of atoms as in the bicrystal for the grain boundary calculation. The total energy of the structure was minimized with respect both to the positions of individual atoms and to the rigid body displacements of the two grains. The grain boundary was maintained under periodic boundary conditions of $2[1\bar{3}0]$ (18.2 Å, two grain boundary structural units long) by 4[001] (11.5 Å) in directions parallel to the grain boundary throughout the calculation. Perpendicular to the grain boundary plane, the calculation block, which was comprised of 50 (310) planes (45.6 Å) on either side of the grain boundary plane, was maintained under a constant pressure, allowing the block to be treated as effectively infinite. These conditions preclude the presence of tensile or compressive stresses normal to the boundary as well as shear stresses parallel to the boundary in the final relaxed structure. Since each calculation can only determine the local minimum energy structure for an initial configuration, determination of the most favored (i.e. global minimum energy) grain boundary structure is only possible by an exhaustive examination of the structures produced from various initial configurations with a given stoichiometry. Calculated grain boundary structures were compared to other structures of the same composition, including a structure in which the grain boundary was stoichiometric (with the lowest energy stoichiometric grain boundary structure) and the point defects were distributed throughout the bulk. Comparison with this latter structure is used to evaluate the possible segregation of point defects to the grain boundary region.

The Monte Carlo method was used to determine the structure and chemistry of the Σ=5 (310) grain boundary at non-zero temperature and at various bulk compositions. The method employed here is the same as that developed by Foiles (30). It utilizes a modified grand canonical ensemble in which the total number of atoms (N), temperature (T), and volume are held constant. The chemical potential difference between the two species ($\Delta\mu=\mu_A - \mu_B$, where μ_A and μ_B are the chemical potentials of species A and B in the AB alloy, respectively) corresponding to a given bulk composition, is also fixed. This last condition ensures that while the ratio of the two species in the block can be altered, the bulk composition far away from the boundary plane remains constant. The actual composition corresponding to a specific value of $\Delta\mu$ was determined by Monte Carlo

calculations on a B2 lattice which measured 6a along each <100> direction, and thus contained 432 atoms, at a temperature of 1000 K. The composition in this simulation block stabilizes after a sufficient number of Monte Carlo steps to the equilibrium composition for this $\Delta\mu$. Many such MC calculations were used to establish a relationship between $\Delta\mu$ and the composition.

Monte Carlo calculations of the Σ=5 (310)[001] grain boundary were performed on an initially stoichiometric grain boundary structure at 1000 K. The unit cell of this structure also had dimensions of $2[1\bar{3}0] \times 4[001]$, and the rigid body displacements between the upper and lower grain were chosen to correspond to those calculated for the minimum grain boundary energy structure in static calculations. While the composition and location of each individual site is allowed to vary, the rigid body displacements remain constant during the Monte Carlo calculations. The calculations were conducted for four bulk compositions: X_{Ni}(bulk)=50.04%, X_{Ni}(bulk)= 51.1%, X_{Ni}(bulk)=53.0%, and X_{Ni}(bulk)= 55.7%.

3. Results and Discussion

3.1 Experimental Image of the NiAl Σ=5 Grain Boundary

The Σ=5 (310) [001] grain boundary was imaged by HREM along the common [001] direction. Figure 1a shows an image of this well-oriented grain boundary. In this orientation, the two grains of B2-ordered NiAl are viewed along columns of pure nickel and pure aluminum. These atomic columns exhibit a white atom contrast at this thickness and defocus (58 Å and -700 Å, respectively), with the columns of nickel atoms brighter than the columns of aluminum atoms. Thus, the image clearly displays the superlattice of the B2-ordered NiAl phase and demonstrates that the chemical ordering of the two grains is continuous up to the grain boundary. Analysis of the image reveals an asymmetry across the grain boundary due to a 1/2 $d_{1\bar{3}0}$ (0.46 Å) rigid body translation of the upper grain towards the right. Further examination reveals that there is also a small expansion of the grain boundary estimated to be 0.18 Å(31).

The structure of this grain boundary can be described in terms of a distorted diamond-shaped structural unit, as shown in Figure 1b. This structural unit has a length of 10 $d_{1\bar{3}0}$(9.1 Å) along the grain boundary and a width of approximately 4 d_{310} (3.6 Å) and displays the 1/2 $d_{1\bar{3}0}$ asymmetry described above. The lattice sites of this structural unit are labelled in order to clarify discussions of the grain boundary; A-D and F are Ni lattice sites and E, G, and H are Al lattice sites.

An important characteristic of this structure, which is also evident in the structural unit schematic, is the close proximity of the atomic sites adjacent to the grain boundary plane. The observed rigid body displacements constrain this near symmetric boundary such that both sites B and C and sites G and H are separated by as little as 1.9 Å, which is only about 2/3 of the matrix separation (between similar atomic types in the B2 lattice) of 2.887 Å. The strong repulsion between layers adjacent to the grain boundary is therefore a dominant factor in determining the grain boundary structure.

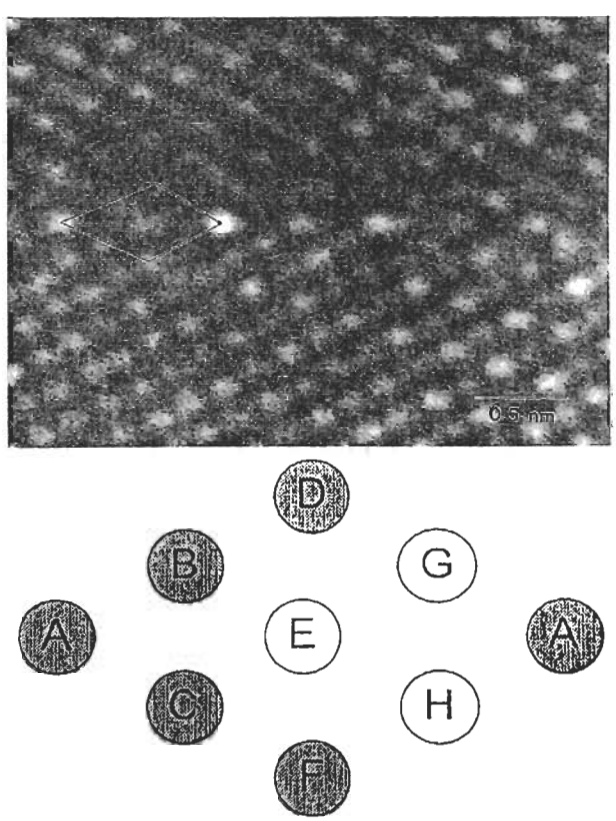

Fig. 1 (a) Experimental image of the well-oriented NiAl Σ=5 (310) [001] grain boundary viewed down the common [001] direction (58 Å thickness and -700 Å defocus) and (b) schematic of the grain boundary structural unit with labelled grain boundary sites. Sites A-D and F lie on the Ni sublattice and sites E, G, and H lie on the Al sublattice.

3.2 Atomistic Calculations at 0K

A large number of atomistic calculations were performed on the stoichiometric Σ=5 (310) [001] grain boundary and on the same boundary containing one point defect per boundary structural unit. These structures were found to relax into a total of 31 different grain boundary structures. The results of these calculations is listed in Table 1 which lists the rigid body displacements parallel to the boundary, Δx, parallel to the boundary and the tilt axis, Δ z, the grain boundary expansion, Δy, and the total energy of the calculation. A total of 36 entries can be found in the table. Calculation number (CN) 1 is the result of relaxation of the structural model originally developed for this boundary based solely on HREM analysis(31). CN6-CN28 are relaxed structures in Ni-rich NiAl containing either a vacancy on an Al site or a Ni antisite defect. CN29-CN36 are relaxed structures in Al-rich NiAl containing either a vacancy on a Ni site or an Al antisite defect. CN6, CN17, CN29 and CN33 are the results of relaxation of a stoichiometric grain boundary (CN2) with defects in the bulk.

The values of the sixth column of Table 1 are plotted in Figure 2. Each bar in the chart represents the total energy calculated at 0K for a given calculation. The value for CN1 indicates that the structure into which the originally proposed structure for this boundary relaxes has a fairly high energy; in Table 1 it can be seen that after relaxation, the rigid body displacements are very different than those experimentally observed, especially Δ y which shows a large grain boundary contraction. This result emphasizes the benefits obtained from a method based on iterative experimentation and theoretical modeling analyses. Examination of the general trends of boundary energy, shows that the grain boundary energy increases with increasing Al content in agreement with the results of Petton and Farkas(21) although the values of the energy are different as expected from the use of different empirical potentials.

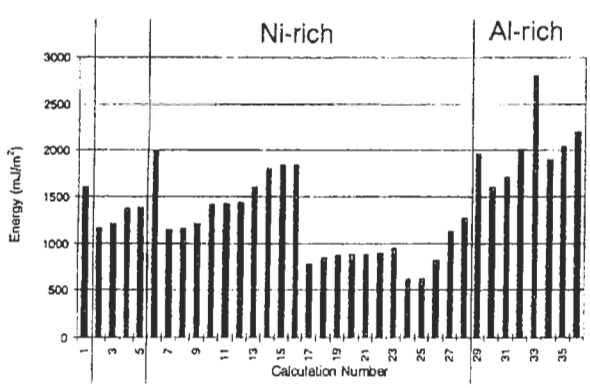

Fig. 2 Plot of the grain boundary energy of each calculated Σ=5 (310) [001] structure (some structures of high energy are omitted). CN1 is the result of the relaxation of a model structure developed solely from prior HREM analysis [Fonda, 1993 #70]. CN2-5: stoichiometric grain boundaries; CN6, 17, 29, 33 are calculations of a stoichiometric boundary, CN2, with Al vacancies, Ni antisite defects, Ni vacancies and Al antisite defects within the bulk, respectively; CN7-16: Ni-rich grain boundaries containing Al vacancies; CN18-28: Ni-rich grain boundaries containing Ni antisite defects; CN30-32: Al-rich grain boundaries containing Ni vacancies; CN 34-36: Al-rich grain boundaries containing Al antisite defects.

3.2.1 Stoichiometric Grain Boundary Structures

Energy minimization of stoichiometric grain boundary structures with various rigid body displacements resulted in only three distinct relaxed grain boundary structures; a fourth calculated structure was determined to be a variant of the highest energy structure. The lowest energy stoichiometric grain boundary structure has a grain boundary energy of 1174 mJ/m^2 (CN 2) and is shown in Figure 4 (a key to the symbols used in figures of grain boundary structures is given in Figure 3) This structure is completely symmetrical (Δ x=0, Δ z=0) and only differs from a geometrically constructed Σ=5 structure in the 0.57 Å grain boundary expansion. As mentioned above, this large grain boundary expansion is due to the close proximity (about 1.9 Å separation) of sites B and C and sites G and H in the geometrical structure. The NiAl effective pair potentials, which show that the Al-Al

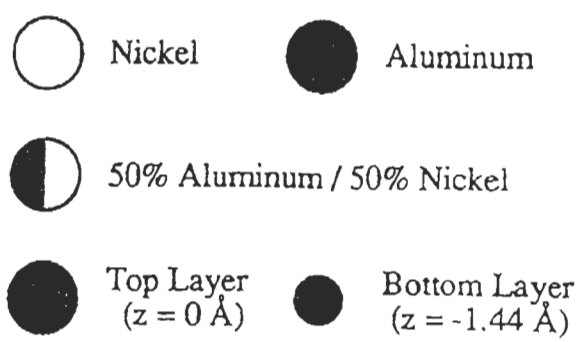

Fig. 3 Key to symbols used in the structure figures.

interactions are strongly repulsive at distances below 2.75 Å while the Ni-Ni interactions are not repulsive until separations below 2.2 Å, demonstrate that this expansion is predominantly caused by interatomic repulsions between the aluminum atoms at sites G and H. The grain boundary expansion which is produced in this structure, in combination with atomic relaxations at the boundary, allow the separation between these two sites to increase to 2.64 Å.

The mirror symmetry evident in the grain boundary structure shown in Figure 4 is removed in the other stoichiometric structures by a rigid body shift in the x direction (along the grain boundary). The next lowest energy grain boundary structure, CN3 is only slightly higher in energy (about 40 mJ/m^2) than the structure in Figure 4. This energy difference is a small fraction of the total grain boundary energy, indicating that this structure may also be observed at stoichiometric grain boundaries. The higher energy stoichiometric structures exhibit a rigid body shift in the z direction (the viewing direction). Such a shift cannot be observed in HREM due to the projection effect in which a three dimensional structure is imaged in two dimensions. The shift of 1/2 lattice parameter in this direction exhibited by the structure CN5 produces a near color mirror across the boundary. This color mirror is slightly distorted by the small rigid body shift in the x direction. The significantly higher energy of this structure suggests that it is a metastable structure whose formation is unlikely.

These stoichiometric grain boundary structures can be used as a basis for comparison with the non-stoichiometric grain boundary structures discussed below. Many of the non-stoichiometric structures are nearly identical to these structures, with the exception of periodically placed point defects at the grain boundary and the minor structural relaxations surrounding them.

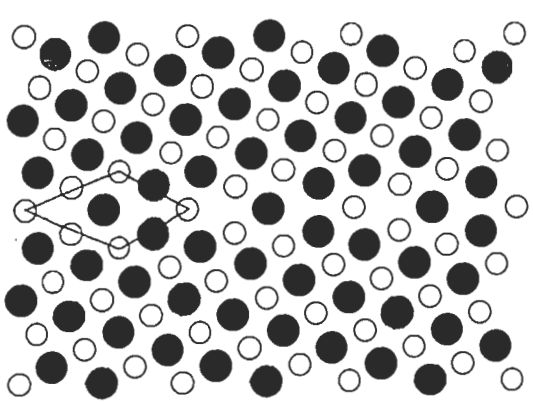

Fig. 4 Calculated structure of the symmetric stoichiometric Σ=5 (310) [001] grain boundary (CN2: E_{GB}=1174 mJ/m^2).

3.2.2 Defects in the Bulk

The lowest energy stoichiometric structure (CN 2) was used to study the energy of point defects within the NiAl grains. An equal number of point defects as present in the relaxed non-stoichiometric structure of interest (see below) were distributed throughout the bulk corresponding to one point defect for each grain boundary structural unit (or for each 26 $Å^2$ of grain boundary area). The change in energy resulting from moving point defects from the bulk to sites at the grain boundary can therefore be determined, revealing the propensity for grain boundary segregation of each type of point defect.

The results of the bulk defect calculations are presented in Figure 5. Comparison of the energy of the structures of CN6 and CN17 clearly show that Ni antisite defects have much lower energy than Al vacancies in Ni-rich NiAl. It is interesting to compare the energies of CN17 with that of CN2 in Figure 2. This clearly shows that adding Ni antisite defects within the bulk will lower the total energy of the calculation below that of stoichiometric NiAl.

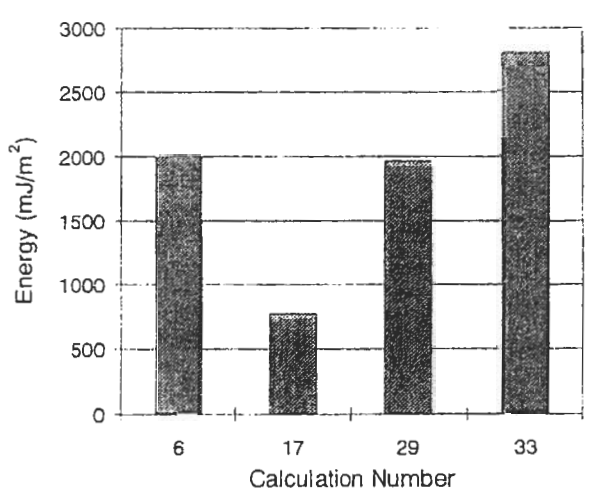

Fig. 5 Comparisons of energies of the four types of point defects within the bulk. CN6, 17, 29, 33 are calculations of a stoichiometric Σ=5 (310) [001] boundary, CN2, with Al vacancies, Ni antisite defects, Ni vacancies and Al antisite defects within the bulk, respectively.

In Al-rich NiAl, it is well known that the point defects in the bulk of aluminum-rich NiAl consist exclusively of constitutional vacancies on the nickel sites instead of aluminum antisite defects(22). The present results are consistent with this data as the energy of an aluminum antisite defect in the bulk is more than the energy of two nickel vacancies. An aluminum antisite defect causes the stoichiometry to change by twice as much as a nickel vacancy. This can be seen in the data of Table 1, where aluminum antisite defects in the bulk (2807 mJ/m^2, CN33) increase the energy by more than twice as much from the energy of a stoichiometric structure (1174 mJ/m^2, CN2) as nickel vacancies in the bulk (1966 mJ/m^2, CN29).

Despite the obvious preference for Ni antisite defects in Ni-rich NiAl and Ni vacancies in Al-rich NiAl, grain boundaries containing all four varieties of defects were relaxed. It is possible that in the environment of the grain boundary, point defects which are not present in the bulk will be energetically feasible due to the reduction of geometrical constraints at the boundary.

3.2.3 Nickel-Rich Grain Boundary Structures

Among the structures containing aluminum vacancies, the lowest energy grain boundary structures (CN7 and CN8) show a decrease in grain boundary energy relative to the stoichiometric boundary, see Figure 2. While these structures were calculated from grain boundaries which initially contained a discrete vacancy at an aluminum site, relaxation of each lattice produced a reconstruction of the boundary which resulted in a more uniform distribution of atoms, see Figure 6 (CN7). These two structures are closely related to the stoichiometric grain boundary structures CN2 and CN3, respectively; compare Figure 6 with Figure 4. They can be derived from these stoichiometric structures either by the removal of an aluminum atom or by the addition of a nickel atom. However, even though the energies of these structures are below those of the stoichiometric structures, the much lower energies of the nickel antisite defect structures (see below) make these structures (and the other aluminum vacancy-containing structures) highly improbable. As can be seen in Figure 2, even structures with nickel antisite defects located in the bulk are energetically favored over any structure which contains aluminum vacancies. Most of the remaining structures which contain aluminum vacancies exhibit obvious aluminum vacancies even after relaxation. The lack of significant relaxation around the aluminum vacancies in these structures results in much higher energies (1400-1850 mJ/m^2) as well as larger grain boundary expansions.

The grain boundaries containing Ni antisite

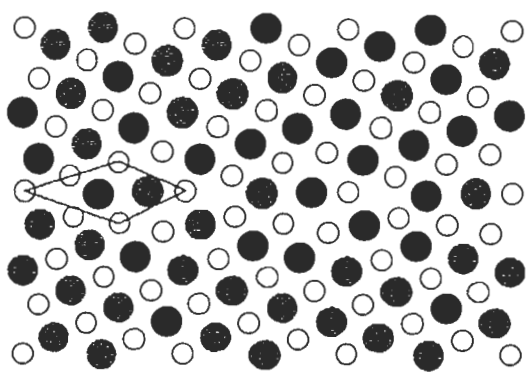

Fig. 6 Calculated structure of a Ni-rich Σ=5 (310) [001] grain boundary which contains vacancies at Al site H. These Al vacancies result in the coalescence of sites G and H (CN7: EGB=1155 mJ/m^2).

defects have the lowest energy of all other boundaries. Within this group of boundaries, the two lowest energy boundaries are CN24 and CN25. Both of these boundaries contain an ordered arrangement of Ni antisite defects in which the defects alternate between sites G and H on successive (001) lattice planes. This arrangement of atoms produces an alternating sequence of Ni and Al atoms in the [001] direction. The origin of the low energy of these boundaries is easily understood from an examination of the effective pair potentials. Alternating the nickel antisite defects with aluminum atoms along an atomic column maximizes the number of low-energy Ni-Al interactions along that column In addition, in CN24 and CN25, the ordering within the two columns is staggered in order to place each antisite defect adjacent to an aluminum atom located across the boundary plane. Thus, while each antisite defect has only six Ni atoms as nearest neighbors (responsible for a slight increase in energy), there are also six second nearest neighbors with which the nickel atom has a strongly attractive interaction. The resultant decrease in energy is evident in the

low (617 and 626 mJ/m^2) grain boundary energies of these structures. A stoichiometric grain boundary with an equivalent number of nickel antisite defects distributed through the bulk has a grain boundary energy of 778 mJ/m^2, CN 17.

The power of the iterative experimental/ theoretical analysis of grain boundary structure relies on a check of the results of the atomistic calculations with the HREM experimental data, in the present case, from the Ni-rich bicrystal. As mentioned above, it is possible to obtain accurate measurements of rigid body displacement both parallel and perpendicular to the boundary from HREM images. Since little variation is seen in the values of grain boundary expansion, Δy, for the Ni antisite containing boundary structures, comparisons will be done based on the Δx values. This comparison is shown for all calculated Ni-rich grain boundary structures in Figure 7. The experimental data is also indicated on the table assuming an accuracy in measurement of 0.2 Å. From the figure, the calculated structures which reproduce the experimental data for this one measurement are CN9, CN10, CN11, CN12, CN18, CN22, CN24 and CN26. Of these calculations, all have significantly higher grain boundary energy than the overall lowest energy structure, CN24, shown in Figure 8. The excellent agreement between this lowest energy structure and the HREM results is strong evidence that this is the correct structure of this particular grain boundary. This consistency between theoretical structural model and experimental data also provided important confirmation of the validity of the new empirical potentials for the further study of other grain boundaries in this alloy (Sections 3.2.1, 3.2.4 and references (17, 28)).

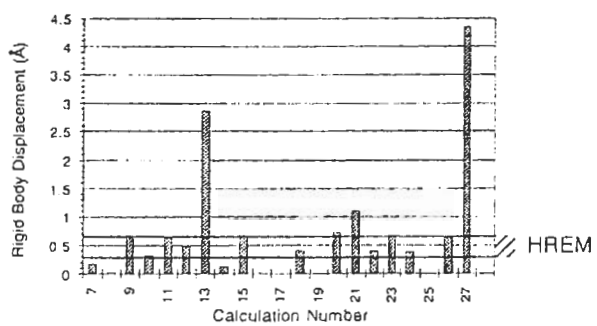

Fig. 7 Plot of the rigid body displacement parallel to the Σ=5 (310) [001] grain boundary plane and perpendicular to the viewing direction (Δx). The horizontal lines represent the limits of experimental accuracy assumed to be +-0.2 Å around the experimentally determined value of 0.46 Å.

3.2.4 Aluminum-Rich Grain Boundary Structures

Structures which contain nickel vacancies at the boundary are similar to the stoichiometric structures (compare Figure 9 (CN31) with Figure 4 (CN2)). The vacancies remain localized at a specific site of the stoichiometric structure, with no significant relaxations of the surrounding atoms. Besides the presence of vacancies, these structures differ from the stoichiometric structures only by smaller rigid body displacements which were enabled by the removal of the Ni atoms.

Atomistic calculations were also performed on structures which contained aluminum antisite defects at the grain boundary. The relaxation of

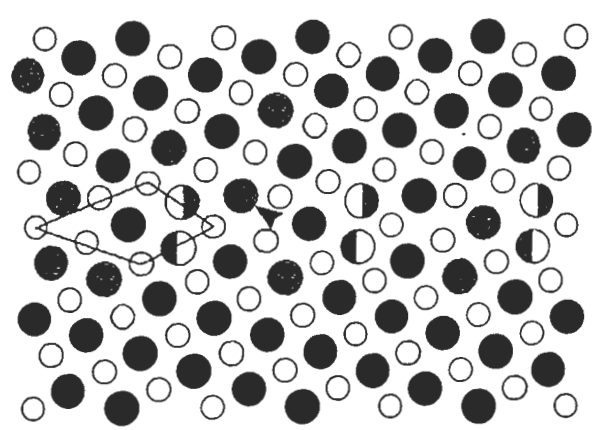

Fig. 8 The lowest energy structure calculated for a Σ=5 (310) [001] grain boundary. This Ni-rich structure contains Ni antisite defects alternating between sites G and H along [001] (CN24: EGB=617 mJ/m^2).

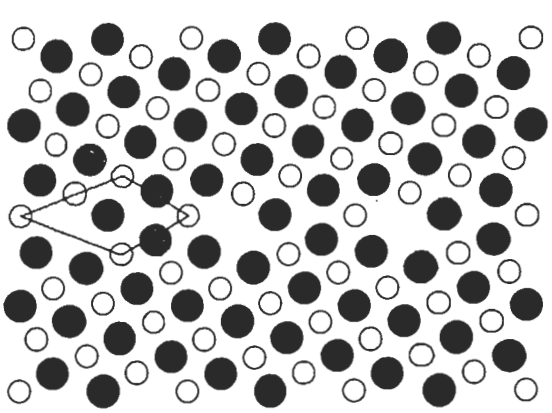

Fig. 9 Calculated structure of an Al-rich Σ=5 (310) [001] grain boundary which contains vacancies at Ni site C (CN31: EGB=1711 mJ/m^2).

geometrical constraints (and an altered chemical environment) at the grain boundary should stabilize these defects at the grain boundary relative to the bulk. As was the case for the structures which contain nickel vacancies, these structures are similar to the calculated stoichiometric structures. The antisite defects are incorporated into the grain boundary structure with only small relaxations surrounding them. In order to compare accurately the energies of these structures which contain aluminum antisite defects to the energies of structures which contain nickel vacancies, it should be recalled that the non-stoichiometric structures in Table 1 and Figure 2 contain a single point defect for each grain boundary repeat unit. Thus the aluminum antisite defect structures deviate from stoichiometry by twice as much as the nickel vacancy structures. In order to make a direct comparison between these energies, one must look at structures which either contain twice the number of nickel vacancies or one-half the number of antisite defects.

In order to make this comparison, the structures of CN34 and CN36 which contain Al antisite defects on grain boundary sites C and A, respectively, were modified to contain only one-half the number of defects, and thus to have the same stoichiometry as the structures with nickel vacancies. This results in a decrease of the calculated grain boundary energy as shown in Figure 10. The energy of structure CN34 decreases to 1553 mJ/m^2; this grain boundary energy is below that of any structure which contains nickel vacancies. Placing the aluminum antisite defects at alternating sites along column A, modified CN36, yields a grain boundary energy of 1662 mJ/m^2, which is comparable to the energies of the lower energy structures which contain nickel vacancies. It is therefore possible that aluminum antisite defects will be present at the grain boundary, with a high concentration at site C and potentially more at site A, in contrast to the predictions of Chen et al.(18). Aluminum antisite defects at site B or within the bulk result in a significantly higher energy and are therefore not expected to be observed. From these data, it is evident that Al-rich NiAl will contain only nickel vacancies in the bulk, as is experimentally observed (22), but that both nickel vacancies and aluminum antisite defects are possible at the grain boundary.

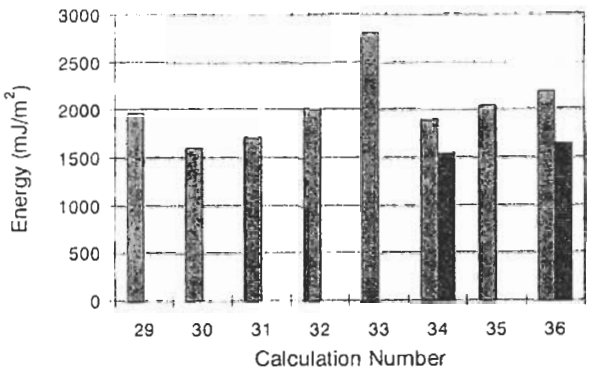

Fig. 10 Comparison of the energies of Al-rich Σ=5 (310) [001] grain boundaries. The second bar for calculations CN34 and CN36 are of modified structures in which the Al antisite defect concentration has been reduced by a factor of two so that the overall stoichiometry is the same as for the calculated structures containing Ni vacancies.

3.2.5 Grain Boundary Segregation Preditions

By comparing the energies of the stoichiometric grain boundary structure with defects within the bulk, the calculations of Section 3.2.2, with the energies of non-stoichometric grain boundaries, Sections 3.2.3 and 3.2.4, the propensity for segregation of the different types of defects to the grain boundary can be analyzied. By examining Figure 2, it can be seen that for every type of defect, at least one non-stoichiometric grain boundary structure can be found which has a lower energy than the corresponding calculation of the stoichiometric grain boundary with the same defect within the bulk. Thus segregation is predicted for certain non-stoichiometric grain boundary structures in all cases although experimental observations of the four cases is impossible since only Ni antisite defects and Ni vacancies will be observed in the bulk of Ni-rich and Al-rich NiAl, respectively.

Of the four types of defects studied, the nickel antisite defect is the only point defect which reduces the energy of the system, when located either at the grain boundary or within the bulk. The energy of a stoichiometric grain boundary with nickel antisite defects within the bulk is only 778 mJ/m^2, CN17, which is almost 400 mJ/m^2 below the 1174 mJ/m^2 grain boundary energy of an undefected stoichiometric boundary, CN2. The only grain boundary structures which have a lower energy than CN17 and therefore favor segregation are the structures of CN24 and CN25 which contain an ordered arrangement of Ni antisite defects

along [001] on the lattice planes adjacent to the grain boundary plane. Structures which contain columns of nickel antisite defects at the grain boundary at a single Al site have higher energies and therefore do not favor segregation.

When an aluminum atom in the bulk is replaced by a nickel atom, there is a slight increase in energy due to the 8 nearest-neighbor interactions (change from Ni-Al to Ni-Ni) and a large (more than 0.15 eV/interaction) decrease in energy due to the 6 next nearest-neighbor interactions (change from Al-Al to Ni-Al). When a string of these replacements occurs along an entire [001] column (either in the bulk or at the grain boundary), two of the next-nearest neighbor interactions become Ni-Ni rather than Ni-Al, resulting in a much smaller energy decrease (nearly 0.3 eV less than for an isolated defect in the bulk). Therefore, structures which contain a column of nickel antisite defects are energetically unfavorable. The maximum fraction of Al atoms in any one column which can be replaced by Ni antisite defects is one-half, with the antisite defects alternating with the remaining Al atoms along the column.

In Al-rich NiAl, segregation of both Ni vacancies and Al antisite defects to the boundary is predicted. However, only Ni vacancies will be present within the bulk. The two lowest energy structures containing Ni vacancies (with E_{GB}= 1606 mJ/m^2, CN30, and 1711 mJ/m^2, CN31, shown in Figure 4) have a much lower energy than the structure with nickel vacancies in the bulk (E_{GB}= 1966 mJ/m^2, CN29). Thus, the nickel vacancies present in the bulk of aluminum-rich alloys will preferentially segregate to the grain boundary. Although segregation of Al antisite defects to the boundary is clearly favored (CN34 vs. CN33, for example), the physically relevant comparison is between the grain boundary with Al antisite defects and the stoichiometric boundary with bulk Ni vacancies. This comparison also clearly favors Al antisite defects at the boundary as can be seen by comparing the energy of the compositionally adjusted CN34, E_{GB}= 1553 mJ/m^2, with CN29, E_{GB}= 1966 mJ/m^2.

With the energy of the Al-rich grain boundary containing an Al antisite defect, modified CN34, E_{GB}= 1553 mJ/m^2, being comparable to the lowest energy boundary containing a Ni vacancy, CN30, E_{GB}= 1606 mJ/m^2, the possibility exists that grain boundaries in Al-rich NiAl may contain Al antisite defects whereas only Ni constitutional vacancies are found in the bulk. The formation of these boundaries requires that the segregation of Ni vacancies to the boundary lead to the creation of an antisite defect. A possible mechanism for this is shown in Figure 11. Two Ni vacancies diffuse to the grain boundary region and occupy sites C and F. The F vacancy then jumps to site H changing the occupancy of site F from Ni to Al. With vacancies on sites C and H, the grain boundary will collapse with site F becoming either site C or site H. The result will now be a boundary structure containing an Al antisite defect on site C.

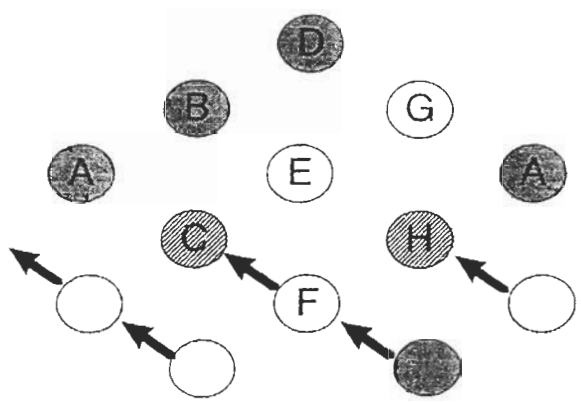

Fig. 11 Mechanism by which the segregation of two Ni vacancies to a Σ=5 (310) [001] grain boundary in Al-rich NiAl can lead to the formation of the lowest energy structure containing Al antisite defects at the boundary site C. The shaded circles represent Ni atoms and the white circles are Al atoms. The segregation of two Ni vacancies to sites C and F is followed by a vacancy jump from the Ni site F to the Al site H. With vacancies on sites C and H (hatched), the structure collapses along the direction of the arrow (or the symmetrically equivalent direction F to H) producing an Al antisite defect on site C. Sites F and H are once again occupied by Ni and Al atoms as at the start of the process.

Referring back to the data in Table 1, a general preference for non-stoichiometric structures in which the point defects occupy sites on the lattice planes adjacent to the grain boundary plane, rather than the grain boundary plane, can be found. In all cases, a grain boundary structure containing the defect on the lattice plane adjacent to the boundary plane has a significantly lower energy that the structure containing the defect at the boundary plane, for

Table 1 Rigid body displacements and calculated grain boundary energies for structures containing one point defect per grain boundary structural unit.

GB structure	Calc. Number	Δ x (Å)	Δ y (Å)	Δ z(Å)	$E_{GB}(mJ/m^2)$	Figure Number
HREM, based on [Fonda and Luzzi, 1993]	1	0.68	-0.38	0.01	1608	
Stoichiometric	2	0	0.57	0	1174	4
Stoichiometric	3	0.43	0.54	0	1213	
Stoichiometric	4	0.74	0.49	1.11	1376	
Stoichiometric	5	0.74	0.53	1.44	1388	
Al vacancy (Ni-rich)						
isolated in bulk	6				2001	
site H	7	0.18	0.02	0	1155	6
sites G and H (alt)	8	0.03	0.83	0	1166	
site G	9	0.62	-0.04	0	1222	
site H	10	0.33	0.34	0	1419	
sites G and H (alt)	11	0.63	0.02	0	1427	
site H	12	0.48	0.19	0	1445	
site H	13	2.88	0.02	1.44	1607	
site E	14	0.13	0.38	1.34	1809	
site G	15	0.69	0.30	0.96	1848	
site H	16	0.01	0.01	0	1849	
Ni antisite (Ni-rich)						
isolated in bulk	17				778	
site H	18	0.41	0.36	0	848	
site H	19	0	0.43	0	877	
site H	20	0.72	0.39	1.01	889	
site H	21	1.10	0.39	1.01	889	
site G	22	0.40	0.35	0	896	
site G	23	0.67	0.39	1.05	954	
sites G and H (alt)	24	0.39	0.36	0	617	8
sites G and H (alt)	25	0	0.43	0	626	
sites G and H (alt)	26	0.64	0.39	0.97	825	
site E	27	4.35	0.47	1.30	1136	
site E	28	0	0.51	0	1275	
Ni vacancy (Al-rich)						
isolated in bulk	29				1966	
site B	30	0.35	0.32	0	1606	
site C	31	0.12	0.47	0	1711	9
site A	32	0.70	0.39	1.05	2014	
Al antisite (Al-rich)						
isolated in bulk	33				2807	
site C	34	0.91	0.62	1.43	1899	
site C	35	0.55	0.73	0	2043	
site A	36	0	0.70	0	2203	

example CN7 vs. CN14, CN24 vs. CN27, CN30 vs. CN32, CN34 vs. CN36. In fact, with one exception, the energies of non-stoichiometric grain boundaries with point defects occupying sites A or E are higher than the energy of the stoichiometric grain boundary with the same defect within the bulk indicating that segregation will not occur to these structures. This trend demonstrates a strong, interesting preference for segregation to a specific plane, but not the grain boundary plane. The one exception, a structure containing an Al antisite defect on site A, CN36, has a lower energy than the calculations of either a Ni vacancy or an Al antisite defect within the bulk, CN29 and CN33, respectively. However, this structure has a higher energy than the structure containing an Al antisite defect on site C, CN34.

3.3 Atomistic Calculations at Room Temperature

The effect of non-stoichiometry in the bulk in Ni-rich NiAl on the structure and composition of the grain boundary was examined by Monte Carlo calculations. The results of these calculations are shown in Figure 12. The layer index indicates the position of each lattice plane, with layer 0 representing the grain boundary plane and the positive and negative layer indices representing the planes above and below the grain boundary plane, respectively. (Site G is contained in layer 1 while site H is contained in layer -1.) The left axis represents the excess concentration of Ni with respect to the stoichiometric composition on each layer (50%) and the right axis is the bulk composition as determined by fixing the chemical potential.

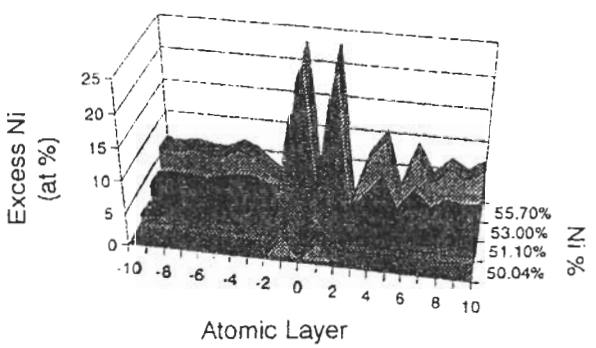

Fig. 12 Plot of the excess Ni at (and near) the Σ=5 (310) [001] grain boundary for bulk compositions of 50.04 % Ni, 51.1% Ni, 53.0% Ni, and 55.7 % Ni as determined from Monte Carlo calculations. Layer indices refer to (310) planes above (+) and below (-) the grain boundary plane. An excess Ni concentration of 25 at. % is equivalent to one-half the Al atoms being replaced by Ni antisite defects.

With increasing bulk Ni concentration, large segregation can be seen to the grain boundary region. However, as predicted from the 0K calculations, segregation to the grain boundary plane is not seen with the excess Ni concentration on layer 0 not changing. Also as predicted, strong segregation is seen to the lattice planes adjacent to the grain boundary plane, layers 1 and -1. The loss of symmetry of the grain boundary structure due to the rigid body displacement parallel to the grain boundary plane is also apparent in the Monte Carlo calculations with the asymmetric distribution of Ni antisite defects on planes near the boundary plane.

These Monte Carlo results are an important confirmation of the stability of the structure calculations. Since the HREM experiments are conducted at room temperature, it is vital to show that important aspects of the relaxed structures produced by molecular statics routines at 0K such as the preferred sites of point defects do not change at higher temperatures.

4. Summary

A synergistic approach utilizing experimental high resolution electron microscopy and N-body atomic structure calculations has been used to determine the atomic structure of a Σ=5 (310) [001] grain boundary in Ni-rich NiAl. The development of a low energy, stable model structure which is consistent with the experimental data confirmed the validity of new empirical potentials for grain boundary calculations in non-stoichiometric NiAl. These potentials were then applied to the study of stoichiometric and non-stoichiometric grain boundary structures to determine the effect and distribution of point defects at the boundaries and the likelihood of defect segregation.

In nickel-rich compositions, although the energies of some structures which contain aluminum vacancies at the grain boundary are significantly below those where the defects are located in the bulk, the much lower energies of structures which contain nickel antisite defects show the antisite defect to be the equilibrium point defect. These nickel antisite defects remain isolated; adjacent antisite defects are higher in energy than isolated defects. The maximum concentration of these defects in a particular atomic column is therefore expected to be 50%, with the nickel antisite defects alternating with the remaining aluminum atoms along that column. This research indicates that nickel antisite defects will segregate weakly to non-adjacent sites neighboring the grain boundary plane but not to the grain boundary plane itself, which will remain free of nickel antisite defects.

Calculations of aluminum-rich compositions confirm that constitutional vacancies at nickel sites accommodate the deviations from stoichiometry in the bulk. There will be a strong segregation of these nickel vacancies to the grain boundary region, where both nickel vacancies and aluminum antisite defects are

predicted. The relative concentrations of these two defects at the grain boundary will depend on the specific atomic structure of the grain boundary.

The lowest energy structure determined from these atomistic relaxation calculations contains nickel antisite defects which alternate between sites G and H along the [001] viewing direction. This structure was also produced by a Monte Carlo calculation of the grain boundary, demonstrating that it is stable at finite temperatures. The Monte Carlo calculations also demonstrated that there is a strong segregation of nickel to these two aluminum sites, even in alloys which are only slightly nickel-rich.

Acknowledgements

The authors would like to thank Prof. V. Vitek for many stimulating discussions. This work was supported by the National Science Foundation (Grant Officer, Dr. Bruce MacDonald) under Grant No. DMR91-11775. One author (MY) was supported by the Department of Energy under Grant No. DE-FG02-87ER45295. Luzzi acknowledges the support of the National Science Foundation under Grant No. INT-94-14511 and the Japanese Society for the Promotion of Science during the writing of the manuscript. Central facilities were supported in part through the National Science Foundation Materials Research Laboratory Program under Grant No. DMR91-20668.

References

1. R. Darolia, Journal of Metals **43**, 44 (1991).
2. K. H. Hahn, K. Vedula, Scripta Metallurgica **23**, 7 (1989).
3. D. F. Stein, L. A. Heldt, in Interfacial Segregation W. C. Johnson, J. M. Blakeley, Eds. (ASM, Metals Park, OH, 1979) pp. 239.
4. T. Ogura, S. Hanada, T. Masumoto, O. Izumi, Metallurgical Transactions **16A**, 441 (1985).
5. T. Takasugi, E. P. George, D. P. Pope, O. Izumi, Scripta Metallurgica **19**, 551 (1985).
6. W. C. Oliver, C. L. White, in High-Temperature Ordered Intermetallic Alloys II N. S. Stoloff, C. C. Koch, C. T. Liu, O. Izumi, Eds. (MRS, Pittsburgh, 1987), vol. 81, pp. 241.
7. C. T. Liu, E. P. George, Scripta Metallurgica **24**, 1285 (1990).
8. E. P. George, C. T. Liu, Journal of Materials Research **5**, 754 (1990).
9. J. J. Kruisman, V. Vitek, J. T. M. D. Hosson, Acta Metallurgica **36**, 2729 (1989).
10. V. Vitek, J. J. Kruisman, J. T. M. D. Hosson, in Interfacial Structure, Properties and Design M. H. Yoo, W. A. T. Clark, C. L. Briant, Eds. (MRS, Pittsburgh, 1988), vol. 122, pp. 139.
11. V. Vitek, S. P. Chen, A. F. Voter, J. J. Kruisman, J. T. M. D. Hosson, in Grain Boundary Chemistry and Intergranular Fracture G. S. Was, S. M. Bruemmer, Eds. (Materials Science Forum, 1989), vol. 46, pp. 237.
12. V. Vitek, S. P. Chen, Scripta Metallurgica **25**, 1237 (1991).
13. A. H. King, M. H. Yoo, in High-Temperature Ordered Intermetallic Alloys C. C. Koch, C. T. Liu, N. S. Stoloff, Eds. (MRS, Pittsburgh, 1985), vol. 39, pp. 99.
14. D. Wolf, K. L. Merkle, in Materials Interfaces: Atomic Level Structure and Properties W. D. a. Y. S., Ed. (Chapman & Hall, London, 1992).
15. R. W. Fonda, M. Yan, D. E. Luzzi, Philosophical Magazine Letters **71**, 221 (1995).
16. M. Yan, S. P. Chen, V. Vitek, in High-Temperature Ordered Intermetallic Alloys VI J. Horton, I. Baker, S. Hanada, R. D. Noebe, D. Schwartz, Eds. (MRS, Pittsburgh, 1995), vol. 364, pp. 455.
17. R. W. Fonda, M. Yan, D. E. Luzzi, Philosophical Magazine A , in press. (1996).
18. S. P. Chen, A. F. Voter, A. M. Boring, R. C. Albers, P. J. Hay, in High-Temperature Ordered Intermetallic Alloys III C. T. Liu, A. I. Taub, N. S. Stoloff, C. C. Koch, Eds. (Materials Research Society, Pittsburgh, 1989), vol. 133, pp. 149.
19. P. P. Camus, I. Baker, J. A. Horton, M. K. Miller, Journal de Physique **40**, C6-329 (1988).
20. M. K. Miller, R. Jayaram, P. P. Camus, Scripta Metallurgica **26**, 679 (1992).
21. G. Petton, D. Farkas, Scripta Metallurgica **25**, 55 (1991).
22. A. J. Bradley, A. Taylor, Proceedings of the Royal Society **A159**, 56 (1937).
23. M. W. Finnis, J. E. Sinclair, Philosophical

Magazine A **50**, 45 (1984).
24. G. J. Ackland, M. W. Finnis, V. Vitek, Journal of Physics F:Metal Physics **18**, L153 (1988).
25. G. J. Ackland, G. Tichy, M. W. Finnis, V. Vitek, Philosophical Magazine A **56**, 735 (1987).
26. J. H. Rose, J. R. Smith, F. Guinea, J. Ferrante, Physical Review B **29**, 2963 (1984).
27. V. Vitek, G. J. Ackland, J. Cserti, in Alloy Phase Stability and Design G. M. Stocks, D. P. Pope, A.G.Giamei, Eds. (MRS, Pittsburgh, 1991), vol. 186, pp. 237.
28. M. Yan, V. Vitek, S. P. Chen, Acta Materialia **44**, 4351 (1996).
29. D. Miracle, Acta Materialia **41**, 649 (1993).
30. S. M. Foiles, Physical Review B **32**, 7685 (1985).
31. R. W. Fonda, D. E. Luzzi, Philosophical Magazine A **68**, 1151 (1993).